Implementation of Individual-based Modelling of Microbial Communities in LAMMPS

NUFEB Modelling Team

15/07/2016

SUMMARY

In this technical report, the details about the biological and physical submodels used in the first version of the Individual-based Model developed by the NUFEB, NUFEB1.0, are presented. The three-dimensional individual-based model is implemented on LAMMPS (a classical molecular dynamics code, and an acronym for Large-scale Atomic/Molecular Massively Parallel Simulator). The details of the model are presented according to the well-known ODD protocol (Overview, Design Concepts and Details) which is a standard protocol for describing Individual-based Models.

TABLE OF CONTENTS

1. INDRODUCTION

The portable water shortage problem is widely discussed and demands a judicial usage of available resources. However, several countries (mostly under-developed and developing) suffer from extreme shortage of the water resources. Waste water treatment plants (WWTP) have served society for several decades now. Activated sludge process treatment plants are the most common types as they provide an advantage of better efficiency and low cost. Management of ASP systems is largely empirical, the ability to predict their behaviour in the light of changes to management is not easy. In effect the behaviour of these systems is driven by the activities of billions of individual microorganisms undertaking metabolism (of the contents of the waste water); growth division and death. Whilst it is easy to predict the behaviour of small populations of microorganisms in controlled small-scale conditions predicting the behaviour of a complete system is not as simple. It is not clear the extent to which system behaviour at the large scale is dependent and can be predicted from the behaviour of the processes operating at the level of the individual bacterium. The present study attempts to model the activated sludge process (ASP) at the individual microbe level, since pilot scale plants and laboratory scale experiments of WWTP are expensive, cumbersome, non-invasive and often cannot provide information at the micro-scale, which is required for operational optimization of WWTP.

The mathematical models used for ASP can be mainly divided in two general classes according to the way the biomass is represented:

I. discrete units/individual particles or
II. a continuum body.

Discrete unit models such as the cellular automaton (Picioreanu et al., 1998a) or individual-based models (Kreft et al., 1998), have been developed and are now becoming widely applied to study effects of spatially multidimensional gradients in biofilms.

Models which use individuals as a basic unit have occasionally been used in ecology since 1970s, but only since the visionary review of Huston et al. (1988) has Individual-based Modelling been an explicitly delineated approach of ecological modelling. 'Individual-based Modelling' refers in the following to simulation models that treat individuals as unique and

discrete entities which have at least one property in addition to age that changes during the life cycle, e.g. weight, rank in a social hierarchy, etc.

For biofilm modelling, Kreft et al. (1998, 2001) initially proposed the Individual-based Modelling (IbM) as a proper tool compared with existing Cellular Automaton (CA) method used for biofilm modelling. In CA models, the biofilm is represented by collection of bricks, in which each brick is represented by a Cartesian grid (Picioreanu et al., 1998a, 1998b, 2000a; Knutson et al., 2005; Tang and Valocchi, 2013, Radu et al. 2010). In IbM, bacterial cells or biomass agents are represented as hard spheres, with each cell/agent having, besides a variable volume and mass, a set of variable growth parameters, position, velocity, genotype etc. The IbM model consists of two parts: one deals with the growth and behaviour of individual bacteria as autonomous agents (i.e., biological processes); the other deals with the substrate and product diffusion and reaction and fluid flow (i.e., physical processes). Each cell grows by consuming the substrate and divides when a certain volume or mass is reached. The pressure build-up due to the growth of biomass is released by maintenance of a minimum distance between the neighbouring cells. In the traditional IbM approach, for each cell, the vector sum of all positive overlap radii with the neighbouring cells, which is called the shoving vector, is calculated and then the position of the cell is shifted in the direction opposite to this vector sum. The substrate concentration is governed by a convection-diffusion-reaction equation and this transport equation is solved in a fixed Cartesian grid. Figure 1 shows the typical computation domain associated with IbM of biofilms. Basically it has three sub-domains each for biofilm, mass transfer boundary layer, and bulk fluid. Numerical simulations in 2D showed that the IbM produced a more confluent and rounded biofilm structures than the CA based models, due to its deterministic and directionally unconstrained spreading of the biomass (Wang and Zhang, 2010).

In NUFEB1.0, the traditional IbM is extended to incorporate mechanical interactions between agents. The model consists of two submodels: biological submodel handles biological processes such as biofilm growth, decay, maintenance, death etc., and physical submodel handles physical processes such as mechanical interactions, deformation, detachment etc. The model is implemented in LAMMPS, an open source C++ molecular dynamics code (http://lammps.sandia.gov/).

2. METHODS

The model is described through the well-known ODD protocol (Overview, Design Concepts and Details) which is a standard protocol for describing Individual based Models (Grimm et al, 2006). Seven elements of ODD which can be grouped into three blocks are shown in Figure 2.

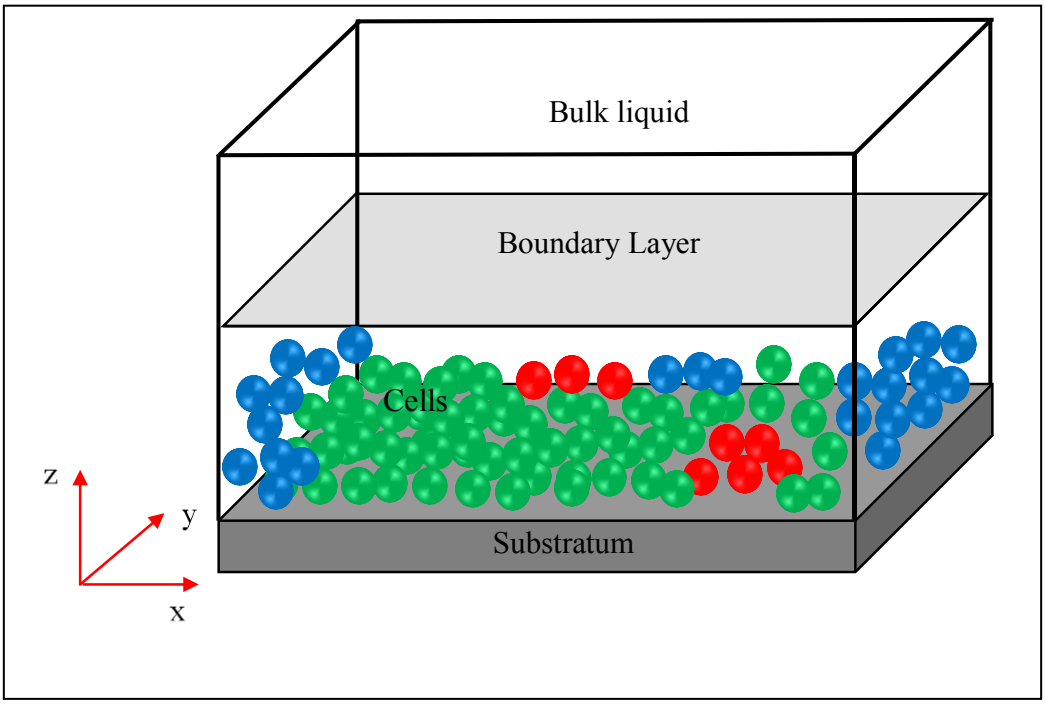

Figure. 1 Computational domain for IbM of biofilms.

Overview	**Purpose**
	State variables and scales
	Process overview and scheduling
Design concepts	**Design concepts**
Details	**Initialization**
	Input
	Submodels

Figure.2 ODD protocol (Grimm et al., 2006).

2.1. Overview

The overview of the model is presented below.

2.1.1 Purpose

A multiscale, multidimensional and multispecies biofilm model based on IbM is developed. The model is intended to use to study activated sludge process in waste water treatments plants. The model considers basic biological processes and mechanical interactions at the first place and the model would be subsequently coupled with OpenFOAM for hydrodynamics.

2.1.2 State variables and scales

A micro scale rectangular volume (rectangular prism) having the dimensions of $L_x \times L_y \times L_z$ representing a sub-space in a macro scale bioreactor is chosen as the computational domain as seen in Figure 3. It can be assumed that the bioreactor volume is made of replicates of the computational domain. The micro and macro scales are coupled through appropriate boundary

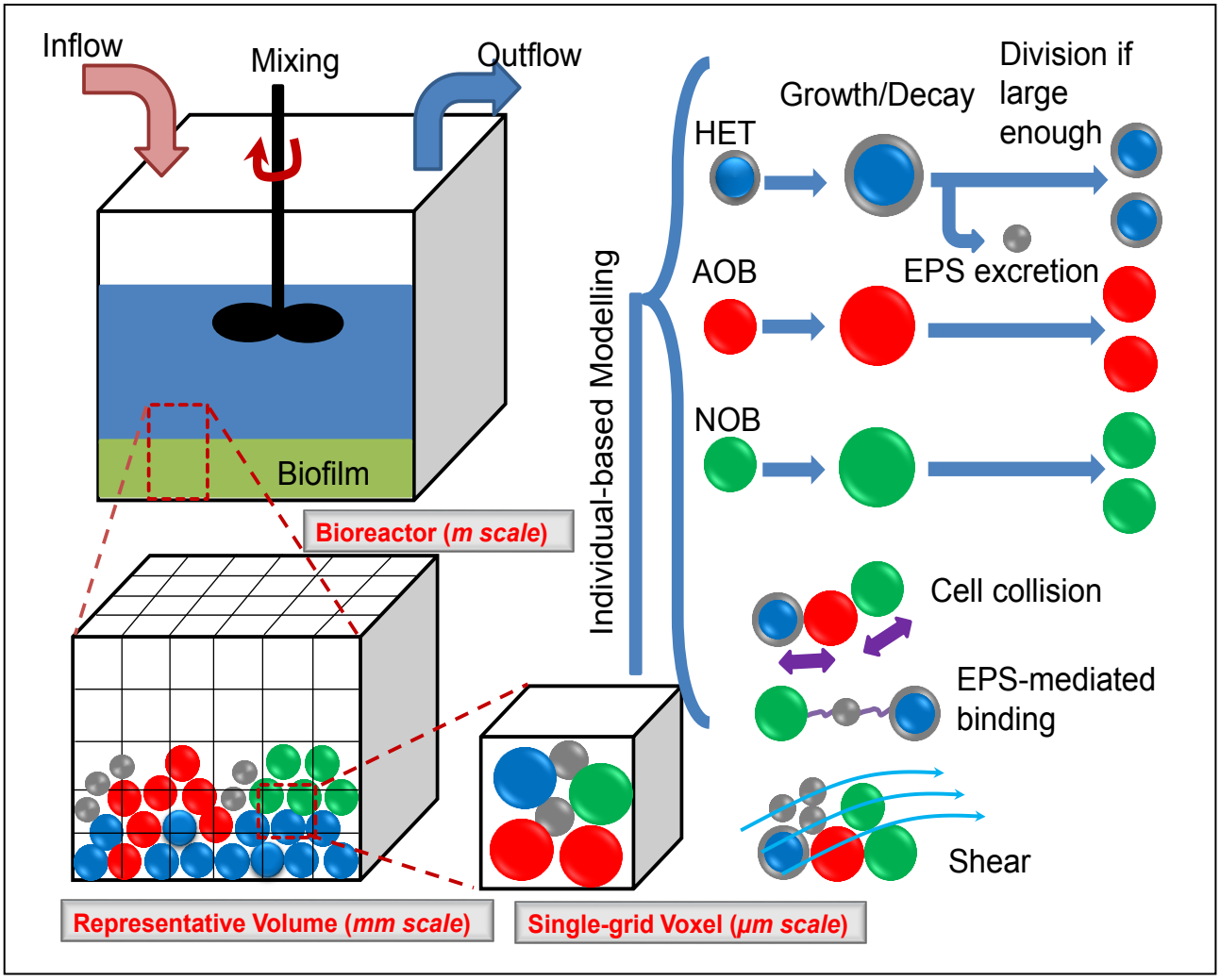

conditions for nutrients.

Figure.3 Summary of the model.

Three functional groups of microorganism and two inert states are considered as agents within the model, these are Heterotrophs-HET, Ammonia oxidizers-AOB, and Nitrite oxidizers-NOB, For the inert states, Extracellular Polymeric Substance-EPS, secreted by some heterotrophs and dead agents are represented by spheres. Agents have four state variables as position, mass, radius, and type. The computational domain is discretised into Cartesian grid cells (voxels). Each voxel has two state variables; position in the overall grid and nutrient concentrations.

2.1.3 Process overview and scheduling

At each biological time step, the following processes are performed sequentially.

I. Nutrient mass balance

Nutrient mass balance for each soluble component (S, NH_4, NO_2, NO_3, O_2) within the spatial unit (box) is computed using a diffusion-reaction equation. In this equation, the reaction term is the net nutrient uptake rate by the particulate components. The diffusion-reaction equation is solved for the steady state solution.

II. Cell growth and division

If the radius of a living agent exceeds a certain threshold, EPS particles are excreted from the HET. If the active mass of HET, AOB, and NOB exceeds a certain threshold (typically, two times the average mass), the mother agent divides into two daughter agents. The mass of each daughter is about 40-60% of the mass of the mother agent.

III. Decay and Maintenance

The rate of decay and maintenance are lumped into one term called decay rate.

IV. Cell death

When agents shrink and reach a certain minimum value, they die, become inert, decay into substrate for use by other agents. The mass of decaying EPS agents also converts to substrate in the same manner. Completely decayed point particles are removed from the simulation.

V. Mechanical relaxation

When agents grow and divide the system deviates from its mechanical equilibrium. Depending on the net force acting on each agent, resulting from its spatial interaction with other local

agents, the position of each agent is updated until the mechanical equilibrium is obtained using the Discrete Element Method (DEM). In DEM, contact, EPS adhesion, shear, and gravitational forces are considered and the position of agents are updated by solving Newton's second law equation.

2.2. Design concepts

Emergence: the IbM is designed such that the spatial pattern of agents and product distribution emerge from local interactions arising from growth, division, death, decay and physical interaction between parcels.

Sensing: in this model, an agent senses the nutrient concentration within the voxel corresponding to its position. The nutrient concentration determines the growth rate of the agent.

Stochasticity: the size of daughter agents after division and positioning of those daughter agents after a division event are the only stochastic processes that we consider in this model.

Observation: at each time step, the state variables for agents and voxels are recorded.

2.3. Details

The details of the model are presented below.

2.3.1 Submodels

Biological and physical processes involved in the system are modelled by different submodels. Those submodels are explained below.

2.3.1.1 Biological processes

I Agents growth/decay

The growth of particulate components (HET, AOB, and NOB) is calculated using the following Monod kinetic equation.

$$\frac{dm_i}{dt} = r_i.m_i \tag{1}$$

Here, m_i is the mass of the particulate component and r_i is the specific growth/decay rate. The specific growth/decay rates for various processes are listed in Table. 1.

Table.1 Growth and decay rates for HET, AOB, NOB, EPS and Dead agents.

Process	**Rate (1/s)**	
Aerobic growth of HET	$\mu_{m,HET}\frac{S_S}{K_{S,HET}+S_S}\frac{S_{O2}}{K_{O2,HET}+S_{O2}}$	R_1
Aerobic growth of AOB	$\mu_{m,AOB}\frac{S_{NH4}}{K_{NH4,AOB}+S_{NH4}}\frac{S_{O2}}{K_{O2,AOB}+S_{O2}}$	R_2
Aerobic growth of NOB	$\mu_{m,NOB}\frac{S_{NO2}}{K_{NO2,NOB}+S_{NO2}}\frac{S_{O2}}{K_{O2,NOB}+S_{O2}}$	R_3
Anoxic growth of HET on NO_3	$\eta_H\mu_{m,HET}\frac{S_S}{K_{S,HET}+S_S}\frac{S_{NO3}}{K_{NO3,HET}+S_{NO3}}\cdot\frac{K_{O2,HET}}{K_{O2,HET}+S_{O2}}$	R_4
Anoxic growth of HET on NO_2	$\eta_H\mu_{m,HET}\frac{S_S}{K_{S,HET}+S_S}\frac{S_{NO2}}{K_{NO2,HET}+S_{NO2}}\cdot\frac{K_{O2,HET}}{K_{O2,HET}+S_{O2}}$	R_5
Decay of HET	b_{HET}	R_6
Decay of AOB	b_{AOB}	R_7
Decay of NOB	b_{NOB}	R_8
Decay of EPS	b_{EPS}	R_9
Decay of Dead	b_X	R_{10}

According to Table 1, the total growth/decay rates for each particulate component are calculated as below:

$$\frac{dm_{HET}}{dt}=\left[(R_1+R_4+R_5)-(R_6)\right]m_{HET}$$

$$\frac{dm_{AOB}}{dt}=\left[(R_2)-(R_7)\right]m_{AOB}$$

$$\frac{dm_{NOB}}{dt}=\left[(R_3)-(R_8)\right]m_{NOB}$$

$$\frac{dm_{EPS,H}}{dt}=\frac{Y_{EPS}}{Y_{HET}}(R_1+R_4+R_5)m_{HET}$$

$$\frac{dm_{EPS}}{dt}=-R_9m_{EPS}$$

$$\frac{dm_D}{dt}=-R_{10}m_D$$

When calculating above growth/decay rates, the nutrient concentrations (S_S, S_{NH4}, S_{NO2}, S_{NO3}, S_{O2}) in the expressions are the nutrient concentration at the voxel (Cartesian grid element) where the particulate component resides.

The above Monod kinetic equation is discretized using an Euler explicit scheme as below:

$$m_i(t+\Delta t_{bio}) = m_i(t) + \Delta t_{bio}.m_i(t) * r_i; i = HET, AOB, NOB, EPS$$

Here, Δt_{bio} is the biological time step (it could be in the order of hours).

II Nutrient uptake rates

The stoichiometric matrix for particulate and soluble components is shown in Table 2. The nutrient uptake rates for each soluble component at each voxel can be calculated by using Tables 1 and 2 as given below.

$$R_S = \left(-\frac{1}{Y_{HET}}\right)R_1 X_{HET} + \left(-\frac{1}{Y_{HET}}\right)R_4 X_{HET} + \left(-\frac{1}{Y_{HET}}\right)R_5 X_{HET} + R_6 X_{HET} + R_7 X_{AOB} + R_8 X_{NOB} + R_9 X_{EPS} + R_{10} X_D$$

$$R_{O2} = \left(-\frac{1-Y_{HET}-Y_{EPS}}{Y_{HET}}\right)R_1 X_{HET} + \left(-\frac{3.42-Y_{AOB}}{Y_{AOB}}\right)R_2 X_{AOB} + \left(-\frac{1.15-Y_{NOB}}{Y_{NOB}}\right)R_3 X_{NOB}$$

$$R_{NH4} = \left(-\frac{1}{Y_{AOB}}\right)R_2 X_{AOB}$$

$$R_{NO2} = \left(\frac{1}{Y_{AOB}}\right)R_2 X_{AOB} + \left(-\frac{1}{Y_{NOB}}\right)R_3 X_{NOB} + \left(-\frac{1-Y_{HET}-Y_{EPS}}{1.17Y_{HET}}\right)R_5 X_{HET}$$

$$R_{NO3} = \left(\frac{1}{Y_{NOB}}\right)R_3 X_{NOB} + \left(-\frac{1-Y_{HET}-Y_{EPS}}{2.86Y_{HET}}\right)R_4 X_{HET}$$

Here, $X_{HET}, X_{AOB}, X_{NOB}, X_{EPS}\, X_D$ are concentrations of HET, AOB, NOB, EPS, and dead agents respectively, at the voxel where the uptake rate is calculated, and they are calculated at voxel (i, j, k) as below.

$$X_{HET}(i,j,k) = \frac{1}{\Delta x.\Delta y.\Delta z}\sum_{p=1}^{N_{HET}} m_{HET,p}$$

$$X_{AOB}(i,j,k) = \frac{1}{\Delta x.\Delta y.\Delta z}\sum_{p=1}^{N_{AOB}} m_{AOB,p}$$

$$X_{NOB}(i,j,k) = \frac{1}{\Delta x.\Delta y.\Delta z}\sum_{p=1}^{N_{NOB}} m_{NOB,p}$$

$$X_{EPS}(i,j,k) = \frac{1}{\Delta x.\Delta y.\Delta z}\sum_{p=1}^{N_{EPS}} m_{EPS,p}$$

$$X_D(i,j,k) = \frac{1}{\Delta x.\Delta y.\Delta z}\sum_{p=1}^{N_D} m_{D,p}$$

Here, N is the No. of respective agents within the voxel (Cartesian grid element), and Δx, Δy, Δz are the dimensions of the voxel.

Table.2 Stoichiometric matrix for particulate and soluble components.

	Particulate Components						**Soluble Components**				
	X_{HET}	X_{AOB}	X_{NOB}	X_{EPS_H}	X_{EPS}	X_D	S_S	S_{O2}	S_{NH4}	S_{NO2}	S_{NO3}
Aerobic growth HET	1			$\frac{Y_{EPS}}{Y_{HET}}$			$-\frac{1}{Y_{HET}}$	$-\frac{1-Y_{HET}-Y_{EPS}}{Y_{HET}}$			
Aerobic growth AOB		1						$-\frac{3.42-Y_{AOB}}{Y_{AOB}}$	$-\frac{1}{Y_{AOB}}$	$\frac{1}{Y_{AOB}}$	
Aerobic growth NOB			1					$-\frac{1.15-Y_{NOB}}{Y_{NOB}}$		$-\frac{1}{Y_{NOB}}$	$\frac{1}{Y_{NOB}}$
Anoxic growth HET on NO_3	1			$\frac{Y_{EPS}}{Y_{HET}}$			$-\frac{1}{Y_{HET}}$				$-\frac{1-Y_{HET}-Y_{EPS}}{2.86Y_{HET}}$
Anoxic growth HET on NO_2	1			$\frac{Y_{EPS}}{Y_{HET}}$			$-\frac{1}{Y_{HET}}$			$-\frac{1-Y_{HET}-Y_{EPS}}{1.71Y_{HET}}$	
Decay HET	-1						1				
Decay AOB		-1					1				
Decay NOB			-1				1				
Decay EPS					-1		1				
Decay Dead						-1	1				

III Agents division

If the mass of the agent (m) reaches a user-defined threshold value, it divides into two daughter agents each with a mass m/2 ± 10%.m. The first daughter agent takes the position of the mother agent while the second daughter agent is placed in a random direction at a distance d (distance between the centres of both agents) corresponding to the diameters of the daughters. The diameters of daughters are calculated using the agent mass and biomass density. Biomass density is constant for each functional group (HET, AOB, and NOB).

2.3.1.2 Physical Processes

I Nutrient mass balance

Nutrient distribution within the rectangular computational domain is calculated by solving diffusion-reaction equation (transport equation) for each nutrient (S, NH_4, NO_2, NO_3, O_2). For any nutrient S, the mass balance is given by,

$$\frac{\partial S}{\partial t} = \nabla . D \nabla S + R$$
$$\nabla = i\frac{\partial}{\partial x} + j\frac{\partial}{\partial y} + k\frac{\partial}{\partial z} \qquad (2)$$

The nutrient uptake rate *R* is calculated in Section (II) above.

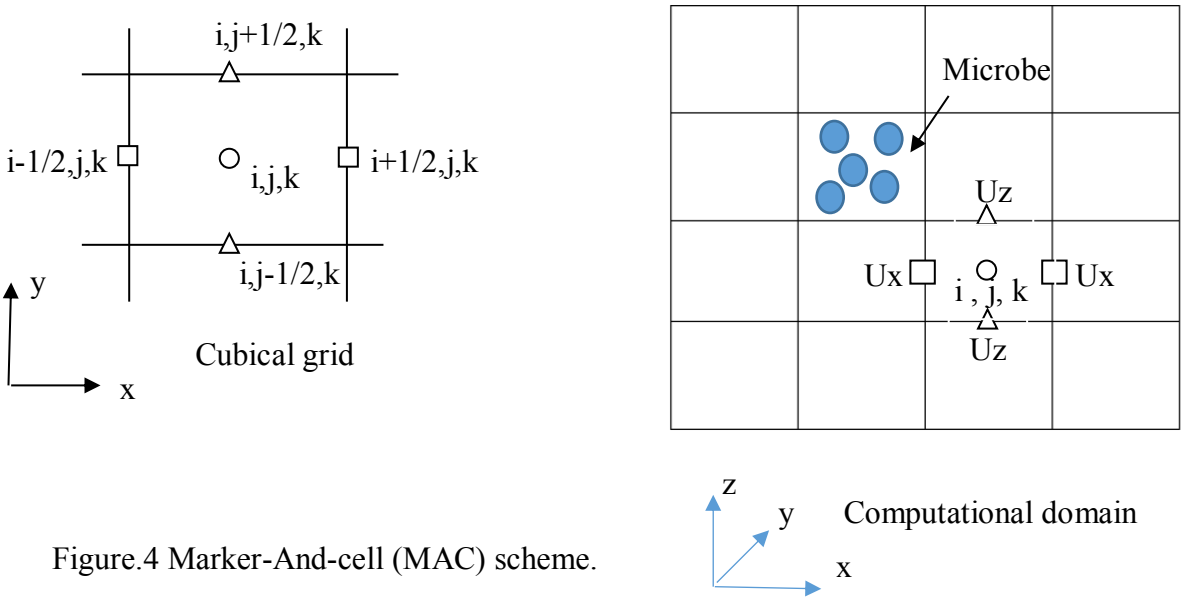

Figure.4 Marker-And-cell (MAC) scheme.

The transport equation is discretized on a Marker-And -Cell (MAC) uniform grid shown in Figure. 4. The scalar S is defined at the centres of the voxel (cubical grid element) and the velocity components U=(U_x, U_y, U_z) are defined at the centres of six faces of the voxel. We do not include the velocity in the present model and so U=0.

The temporal derivative and spatial derivatives of the transport equation are discretized by Forward Euler and Central Finite Differences, respectively. For a given nutrient concentration field at time t, the concentration field at next time step can be calculated using following discretized equations.

$$\frac{S_{i,j,k}^{n+1}-S_{i,j,k}^{n}}{\Delta t}=\frac{Jx_{i+1/2,j,k}-Jx_{i-1/2,j,k}}{\Delta x}+\frac{Jy_{i,j+1/2,k}-Jy_{i,j-1/2,k}}{\Delta y}+\frac{Jz_{i,j,k+1/2}-Jz_{i,j,k-1/2}}{\Delta z}+R_{i,j,k}$$

$$Jx_{i+1/2,j,k}=D_{i+1/2,j,k}\frac{S_{i+1,j,k}^{n}-S_{i,j,k}^{n}}{\Delta x};Jy_{i,j+1/2,k}=D_{i,j+1/2,k}\frac{S_{i,j+1,k}^{n}-S_{i,j,k}^{n}}{\Delta y};Jz_{i,j,k+1/2}=D_{i,j,k+1/2}\frac{S_{i,j,k+1/2}^{n}-S_{i,j,k}^{n}}{\Delta z}$$

$$\overline{Ux}_{i,j,k}=\frac{Ux_{i+1/2,j,k}+Ux_{1-1/2,j,k}}{2};\overline{Uy}_{i,j,k}=\frac{Uy_{i,j+1/2,k}+Uy_{1,j-1/2,k}}{2};\overline{Uz}_{i,j,k}=\frac{Uz_{i,j,k+1/2}+Uz_{1,j,k-1/2}}{2}$$

$$S_{i,j,k}^{n}=S(i,j,k,t=n\Delta t);S_{i,j,k}^{n+1}=S(i,j,k,t=(n+1)\Delta t)$$

II Mechanical relaxation

When agents grow and divide the system deviates from mechanical equilibrium and hence mechanical relaxation is needed to update the positions of the agents and minimize the internal mechanical energy of the system. The mechanical relaxation is done using the Discrete Element Method (DEM). In DEM, the Newtonian equation of motion is solved for each particle in a Lagrangian framework (Cundall and Strack, 1979) which updates the position of the particle. The equations for the translational and rotational movement is given by:

$$\begin{aligned} m_i\frac{d\vec{v}_i}{dt}&=\vec{F}_i=\vec{F}_{c,i}+\vec{F}_{f,i}+\vec{F}_{a,i}+\vec{F}_{g,i}\\ I_i\frac{d\vec{\omega}}{dt}&=T_i \end{aligned} \tag{3}$$

where $\vec{v}_i,\vec{\omega}_i,m_i,I_i,\vec{F}_i,\vec{T}_i$ are the translational velocity, rotational velocity, mass of the agent, moment of inertia of the agent, the net force, and the net torque, respectively.

The net force acting on an agent is calculated as the sum of the contact, adhesion, gravitational, and fluid forces acting on the agent. The contact force ($\vec{F}_c$) is calculated as the sum of all the forces due to interaction with neighbouring agents. The adhesive force ($\vec{F}_a$) is calculated as a sum of all pair-wise adhesive interaction due to the EPS. The fluid-particle interaction force ($\vec{F}_f$) is obtained from a drag model. The gravitational force is $\vec{F}=m\vec{g}$, where $\vec{g}$ is the gravitational acceleration.

The following steps are enlisted to solve the dynamics of agents.

a. Neighbour list building

Neighbouring agents that are in actual contact or in the vicinity of each other, are identified using the agents' positions information.

b. Contact model

This model calculates the forces due to inter-agent collisions and energy dissipation due to the frictional and viscous damping. In the present work, a linear spring-dashpot model is employed for the contact force model with the static friction between the particles, modelled according to the Coulomb's law.

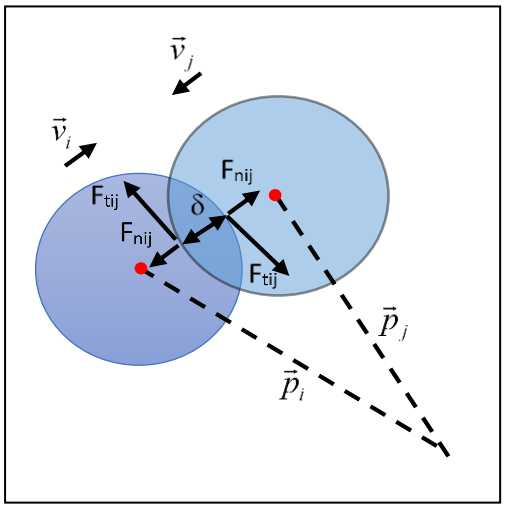

Figure 5. A schematic showing two particles i and j are in contact. Particle position (p), velocity (v), overlap distance (δ), normal and tangential forces (F) are shown.

The normal and tangential forces are given below.

$$\vec{F}_{nij} = f(\delta_{ij}/d)(k_n \delta_{ij} \vec{n}_{ij} - \gamma_n m_{eff} \vec{v}_{nij})$$
$$\vec{F}_{tij} = f(\delta_{ij}/d)(-k_t \vec{\delta}_{tij} - \gamma_t m_{eff} \vec{v}_{tij}) \quad (4)$$
$$\vec{F}_{c,i} = \sum_{j=1}^{N} (\vec{F}_{nij} + \vec{F}_{tij})$$

where $k_{n,t}$ and $\gamma_{n;t}$ are the spring stiffness and viscoelastic constants, respectively, and $m_{eff} = m_i m_j/(m_i + m_j)$ is the effective mass of spheres with masses m_i and m_j. The corresponding contact force on particle j is simply given by Newton's third law, i.e $\vec{F}_{ji} = -\vec{F}_{ij}$. The function f $(\delta_{ij}/d) = 1$ is for the linear spring-dashpot model, and f $(\delta_{ij}/d) = \sqrt{\delta_{ij}/d}$ is for Hertzian contacts with viscoelastic damping between spheres. Here d is the distance between two centres of interacting particles. N is the total number of neighbours.

The particle-wall contact forces are also calculated as above and in this case the wall is considered as a particle having a radius of infinity.

c. Adhesion model

The mass of EPS plays a role in the adhesion force between the particulate agents. The EPS link between the particles are treated as much more stiffer springs, but only employing the attractive forces. Total effective EPS mass is calculated between the agents (m_{ij}^{eps}) and then a spring stiffness is defined per unit mass (k^{eps}). The EPS forces between two agents are calculated according to the effective spring stiffness ($k^{eps} m_{ij}^{eps}$) multiplied by the gap between two agents. A fairly similar approach was first suggested by Head et al. (2013) to produce a mechanically stable biofilm.

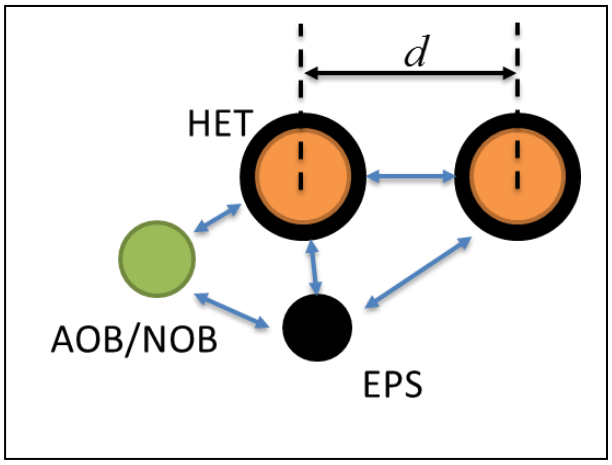

Figure 6. A schematic showing agent-agent interactions.

The EPS-mediated binding forces are then calculated as

$$\vec{F}_{eps,ij} = k^{eps} m_{ij}^{eps} (d_{ij} - d_{0ij}).\frac{\vec{d}_{ij}}{d_{ij}}$$
$$\vec{F}_{a,i} = \sum_{j=1}^{N} \vec{F}_{eps,ij} \quad (5)$$

Here d_{0ij} is the sum of the radii of two interacting agents.

d. Drag model

The coupling between fluid and particles is assumed as only one-way. All agents can be disturbed by the fluid flow, but the fluid is not disturbed by the presence of particulate agents. In this work, the drag model is based on Stokes flow passing a sphere, and it is given by

$$\vec{F}_{f,i} = 6\pi.\mu.r_i\ .\vec{v}(\vec{x}_i) \quad (6)$$

where $\mu, r_i, \vec{v}$ are fluid dynamic viscosity, radius of the particle, and fluid local velocity relative to the particle, respectively.

2.3.2 Input parameters

The input parameters can be taken from the literature and defined in the input script. See the user manual for how the parameters are defined in the input script. A list of typical input parameters are shown in Table 3.

2.3.3 Initialization

The initial nutrient concentrations and the initial agents can be described in the input script and data file, respectively. See the user manual for more information.

3. EXAMPLES

Some examples are presented for floc/biofilm morphology and shear induced deformation.

3.1 Flocs/biofilm morphology

The diffusion-reaction equation Eq. (2) is modelled as a non-dimensional process using appropriate reference values for nutrient concentrations, length, time, and biomass. We then obtain the following non-dimensional equation.

$$\frac{\partial S^*}{\partial t^*} = \delta^2 \nabla^2 S^* + R^* \tag{7}$$

where S^*, R^*, and t^* are non-dimensional nutrient concentration, uptake rate, and time. The non-dimensional parameter, $\delta = \sqrt{S_{bulk}.D.Y_s \Big/ \mu_{\max} \rho L^2}$.

Here, $S_{bulk}, D, Y_s, \mu_{\max}, \rho, L$ are the bulk nutrient concentration, diffusion coefficient, yield coefficient, maximum specific growth rate, biomass density, and boundary layer thickness, respectively. The parameter δ represents the ratio between the nutrient transport to the biomass and the nutrient consumption by the bacteria and δ is also considered as a proxy for the active layer thickness of the floc/biofilm. The active layer is where the nutrient can penetrate into the biomass and hence the bacteria can grow relatively fast compared to the rest of the cells.

Tabel.3 Parameters

Parameters	Symbol	Value	Unit	Reference
Computational domain				
Dimensions	$L_x x L_y x L_z$	100x100x100	μm^3	-
Cartesian grid cells	$N_x x N_y x N_z$	10x10x10	-	-
Kinetic and stoichiometric				
Maximum specific growth rate for HET	$\mu_{m,HET}$	6	d^{-1}	Henze et al. (1999)
Maximum specific growth rate for AOB	$\mu_{m,AOB}$	0.76	d^{-1}	Rittmann and McCarty (2001)
Maximum specific growth rate for NOB	$\mu_{m,NOB}$	0.81	d^{-1}	Rittmann and McCarty (2001)
Decay rate of HET	b_{HET}	0.4	d^{-1}	Henze et al. (1999)
Decay rate of AOB	b_{AOB}	0.11	d^{-1}	Rittmann and McCarty (2001)
Decay rate of NOB	b_{NOB}	0.11	d^{-1}	Rittmann and McCarty (2001)
Decay rate of EPS	b_{EPS}	0.17	d^{-1}	Ni et al. (2009)
Dissolved oxygen affinity for HET	$K_{O2,HET}$	0.81	kgm^{-3}	Wanner et al. (2006)
Carbon source affinity for HET	$K_{S,HET}$	$1x10^{-2}$	kgm^{-3}	Wanner et al. (2006)
Nitrite affinity for HET	$K_{NO2,HET}$	$3x10^{-4}$	kgm^{-3}	Wanner et al. (2006)
Nitrate affinity for HET	$K_{NO3,HET}$	$3x10^{-4}$	kgm^{-3}	Wanner et al. (2006)
Dissolved oxygen affinity for AOB	$K_{O2,AOB}$	$5x10^{-4}$	kgm^{-3}	Rittmann and McCarty (2001)
Ammonia affinity for AOB	$K_{NH4,AOB}$	$1x10^{-3}$	kgm^{-3}	Rittmann and McCarty (2001)
Dissolved oxygen affinity for NOB	$K_{O2,NOB}$	$6.8x10^{-4}$	kgm^{-3}	Rittmann and McCarty (2001)
Nitrite affinity for NOB	$K_{NO2,NOB}$	$1.3x10^{-3}$	kgm^{-3}	Rittmann and McCarty (2001)
Yield coefficient for HET growth	Y_{HET}	0.61	g_{COD}/g_{COD}	Ni et al. (2009)
Yield coefficient for AOB growth	Y_{AOB}	0.33	g_{COD}/g_N	Rittmann and McCarty (2001)
Yield coefficient for NOB growth	Y_{NOB}	0.083	g_{COD}/g_N	Rittmann and McCarty (2001)
EPS formation coefficient	Y_{EPS}	0.18	g_{COD}/g_{COD}	Ni et al. (2009)
Yield of inert biomass	Y_I	0.4	g_{COD}/g_{COD}	Alpkvist et al. (2006)
Reduction factor in anoxic conditions	η_{HET}	0.6	-	Henze et al. (1999)
Nutrient transfer				
Diffusion coefficient for oxygen	D_{O2}	$1.73x10^{-4}$	m^2d^{-1}	Alpkvist et al. (2006)
Diffusion coefficient for ammonia	D_{NH4}	$1.21x10^{-4}$	m^2d^{-1}	Alpkvist et al. (2006)
Diffusion coefficient for nitrite	D_{NO2}	$1.04x10^{-4}$	m^2d^{-1}	Alpkvist et al. (2006)
Diffusion coefficient for nitrate	D_{NO3}	$1.04x10^{-4}$	m^2d^{-1}	Alpkvist et al. (2006)
Diffusion coefficient for carbon	D_S	$4.32x10^{-5}$	m^2d^{-1}	Alpkvist et al. (2006)
Substrate boundary concentration	$S_{S,BC}$	0.04	$kg_{COD}\ m^{-3}$	-
Ammonia boundary concentration	$S_{NH4,BC}$	0.04	$kg_N\ m^{-3}$	-
Nitrite boundary concentration	$S_{NO2,BC}$	0.001	$kg_N\ m^{-3}$	-
Oxygen boundary concentration	$S_{NO3,BC}$	0.005	$kg_N\ m^{-3}$	-
Oxygen boundary concentration	$S_{O2,BC}$	0.005	kgm^{-3}	-
Mechanics				
Normal contact stiffness	k_n	$2x10^{-4}$	Nm^{-1}	-
Normal contact viscous constant	γ_n	$5x10^{-5}$	s^{-1}	-
EPS stiffness per unit EPS mass	k^{eps}	$5x10^9$	s^{-2}	Head (2013)
Dynamics viscosity	μ	0.001	Pa.s	Head (2013)

Figure 7 shows a biofilm and the nutrient available for each agent. It is seen that the nutrient is depleted towards the bottom of the biofilm. The agents on the top layer of the biofilm would grow fast compared to the rest of the agents and hence this top layer is called the active layer.

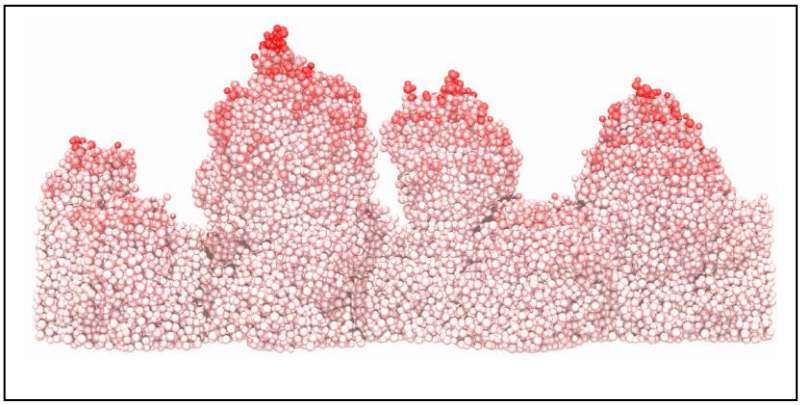

Figure 7. Nutrient available for each agent. The active layer is obvious on the top of the biofilm.

When δ increases the nutrients would penetrate deeper into the biofilm and hence the active layer thickness also increases. When active layer thickness increases the heterogeneity within the biofilm would decrease and hence the biofilm/floc surface would be smooth. On the other hand, smaller active layer thickness would increase the heterogeneity in the biofilm due to steeper nutrient gradients across the biomass and hence higher heterogeneity together with stochasticity would result in a rough surface for the biofilm/floc as can be seen in Figure 8.

3.2 Shear induced deformation

Shear induced deformation of a floc or aggregate or biofilm can be studied by using the drag model mentioned above (Eq. 6). A linear velocity profile is applied on an aggregate having HET (blue) and EPS (grey) as seen in Figure 9. The initial aggregate deforms and finally breaks into two parts. The two parts are not identical in this case due to the heterogeneity of EPS distribution and hence non-uniform mechanical strength of the aggregate.

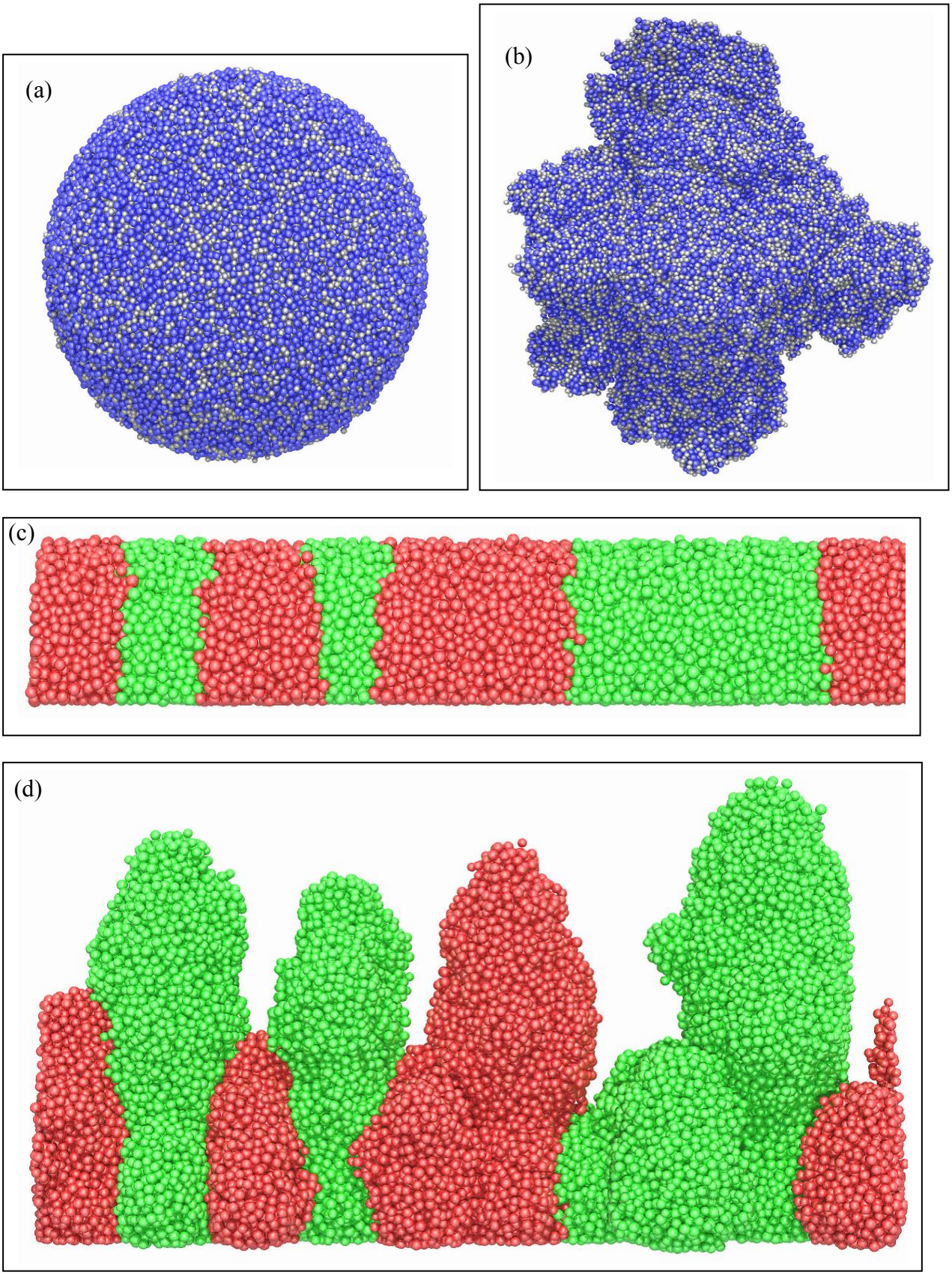

Figure 8. Floc/Biofilm growth at high and low δ: (a) Floc at high δ; (b) Floc at low δ; (c) Biofilm at high δ; (d) Biofilm at low δ.

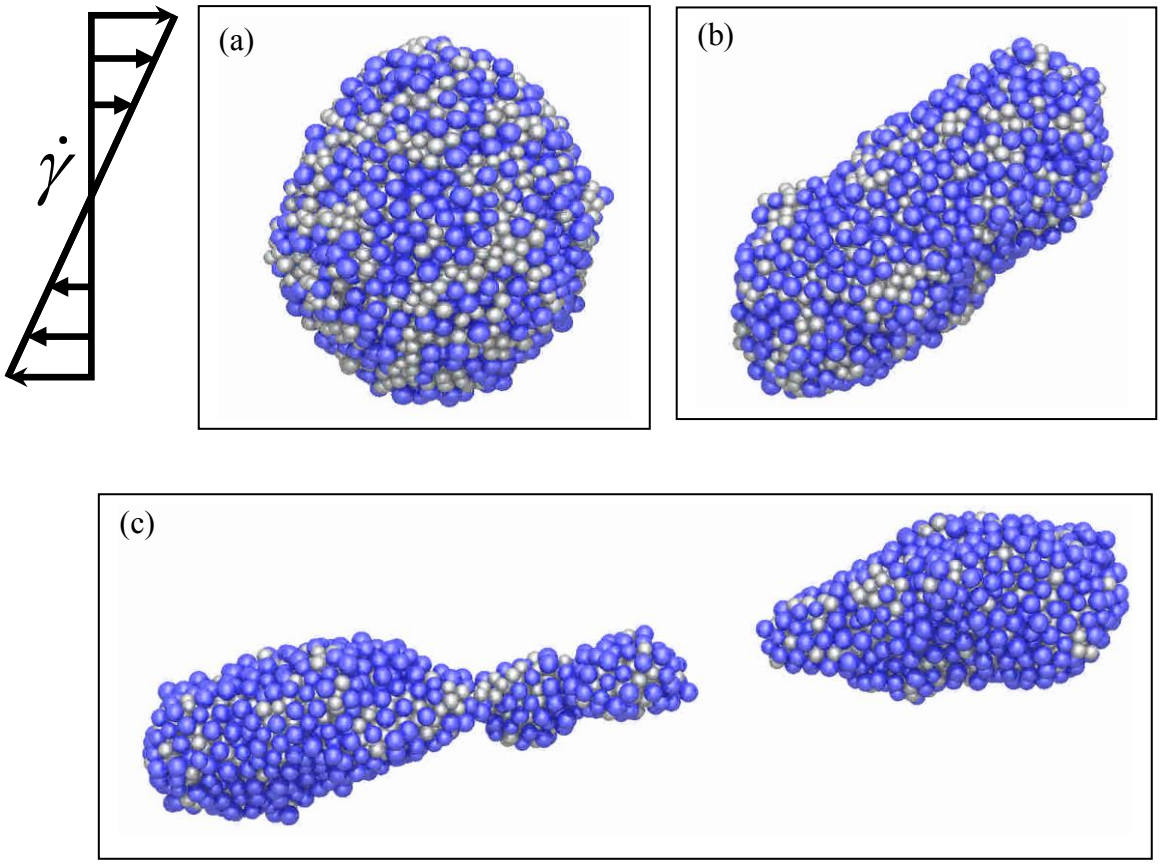

Figure 9. Aggregate deformation at shear rate $\dot{\gamma}$: (a) Initial; (b) Deformation; (c) Detachment.

REFERENCES

Alpkvist, E., Picioreanu, C., van Loosdrecht, M.C.M., Heyden, A., (2006). Three-dimensional biofilm model with individual cells and continuum EPS matrix. Biotechnology & Bioengineering 94 (5), 961-979.

Cundall, P.A. and Strack, O.D.L., (1979). A discrete numerical model for granular assemblies. Geotechnique 29(1), 47-65.

Grimm et al. (2006). A standard protocol for describing individual-based and agent-based models. Ecological Modelling 198, 115-126.

Head, D.A., (2013). Linear surface roughness growth and flow smoothening in a three-dimensional biofilm model. Physical Review E: Statistical, Nonlinear, and Soft Matter Physics 88 (3), 032702.

Henze, M., Gujer, W., Mino, T., Matsuo, T., Wentzel, M.C., Marais, G.V.R., Van Loosdrecht, M.C.M., (1999). Activated sludge model No.2d, ASM2d. Water Science & Technology 39 (1), 165-182.

Huston, M., DeAngelis, D., Post, W., (1988). New computer models unify ecological theory. BioScience 38, 682-691.

Kreft, J.-U. Booth, G., Wimpenny, J.W.T., (1998). BacSim, a simulator for individual-based modelling of bacterial colony growth. Microbiology 144, 3275-3287.

Kreft, J.U., Picioreanu, C., Wimpenny, J.W.T., Van Loosdrecht, M.C.M., (2001). Individual-based modelling of biofilms. Microbiology 147, 2897–2912.

Knutson, C.E., Werth, C.J., Valocchi, A.J., (2005). Pore-scale simulation of biomass growth along the transverse mixing zone of a model two-dimensional porous medium. Water Resources Research 41, W07007.

Ni, B.-J., Fang, F., Xie, W.-M., Sun, M., Sheng, G.-P., Li, W.-H., Yu, H.-Q., (2009). Characterization of extracellular polymeric substances produced by mixed microorganisms in activated sludge with gel-permeating chromatography, excitation-emission matrix fluorescence spectroscopy measurement and kinetic modelling. Water Research 43 (5), 1350-1358.

Ofiteru, I.D., Bellucci, M., Picioreanu, C., Lavric, V., Curtis, T.P., (2014). Multi-scale modelling of bioreactor separator system for wastewater treatment with two-dimensional activated sludge floc dynamics. Water research 50, 382-395.

Picioreanu, C., van Loosdrecht, M.C.M., Heijnen, J.J., (1998a). A new combined differential-discrete cellular automaton approach for biofilm modelling: application for growth in gel beads. Biotechnology & Bioengineering 57 (6), 718-731.

Picioreanu, C., van Loosdrecht, M.C.M., Heijnen, J.J., (1998b). Mathematical modeling of biofilm structure with a hybrid differential-discrete cellular automaton approach. Biotechnology & Bioengineering 58 (1), 101-116.

Picioreanu, C., van Loosdrecht, M.C.M., Heijnen, J.J., (2000). Effect of diffusive and convective substrate transport on biofilm structure formation: a two-dimensional modeling study. Biotechnology & Bioengineering 69 (5), 504-515.

Radu, A.I., Vrouwenvelder, J.S., van Loosdrechta, M.C.M., Picioreanu, C., (2010) Modelling the effect of biofilm formation on reverse osmosis performance: Flux, feed channel pressure drop and solute passage. Journal of Membrane Science 365, 1–15.

Rittmann, B.E., McCarty, P.L., (2001). Environmental Biotechnology: Principles and Applications. McGraw-Hill Book Co., Singapore.

Schulenburg, D.A.G., Pintelon, T. R. R., Picioreanu, C., Loosdrecht, M. C. M. V, Johns, M.L., (2009). Three-Dimensional Simulations of Biofilm Growth in Porous Media. AIChE Journal 55, 494-504.

Tang, Y. and Valocchi, A.J., (2013). An improved cellular automaton method to model multispecies biofilms. Water research 47, 5729 -5742.

Wang, Q. and Zhang, T., (2010). Review of mathematical models for biofilms. Solid State Communications 150, 1009-1022.

Wanner, O., Eberl, H., Morgenroth, E., Noguera, D., Picioreanu, C., Rittmann, B., van Loosdrecht, M.C.M., (2006). Mathematical Modeling of Biofilms. IWA Publishing, London.